PHYSICAL REVIEW B VOLUME 48, NUMBER 4 15 JULY 1993-II

Quantitative measurement of residual biaxial stress by Raman spectroscopy in diamond grown on a Ti alloy by chemical vapor deposition

Joel W. Ager III and Michael D. Drory*
Center for Advanced Materials, Materials Sciences Division, Lawrence Berkeley Laboratory, University of California, Berkeley, California 94720
(Received 5 February 1993)

Raman spectroscopy is used to study residual stress in diamond grown on Ti–6Al–4V by chemical vapor deposition. A general model is developed to use Raman spectroscopy to measure biaxial stress in polycrystalline, diamond-structure films. The as-grown film has 7.1 GPa of residual compressive stress, consistent with the difference in thermal-expansion coefficients between the diamond film and the substrate. Examination of the Raman spectra of the film in the vicinity of Brale indentations reveals that residual stresses in the film of up to approximately 17 GPa can be accommodated in the film before delamination occurs.

I. INTRODUCTION

The potential of chemical vapor deposited (CVD) diamond as an engineering material stems from its extreme properties which include the highest hardness, Young's modulus, and room-temperature thermal conductivity of any known material as well as a low coefficient of friction.[1–3] Exploiting these attractive features in thin-film applications requires that films can be deposited with adequate adhesion to the substrate. In this regard, the presence of residual stress is an important aspect of film reliability, which has been studied in a number of thin-film systems.[4] However, reliability issues which pertain to diamond coatings remain largely unexplored.

Residual stress in brittle films on sufficiently brittle substrates is a superposition of a thermal component due to a thermal-expansion mismatch between the film and substrate (during cooling from the deposition temperature) and an "intrinsic" component due to the processing.[5] The sign of stress may be compressive or tensile, depending on the film and/or substrate materials and processing conditions. For example, Knight and White[6] have estimated CVD diamond film stresses of 5.5 GPa (compressive) on alumina and 2.1 GPa (tensile) on TiC. Residual film stress may result in a lower mechanical reliability of the film arising from a number of failure mechanisms, such as film splitting and spallation, and substrate cracking.[7] A quantative measure of film stress is necessary both for the understanding of these reliability issues and for the design of useful CVD diamond materials.

The measurement of residual stress in CVD diamond has been the focus of several previous studies employing a number of techniques, such as thin substrate deformation,[5,8] vibrating membrane analysis,[9] and Raman spectroscopy.[6,10,11] These studies have focused on CVD diamond on Si (polycrystalline growth),[5,6,8,11] or c-BN (epitaxial growth).[10] Previous Raman studies have either interpreted the stress-induced shifts in diamond Raman frequency in terms of a *hydrostatic* stress model[6] or a *biaxial* stress model[10,11] developed originally to study stress in Si(100) grown epitaxially on sapphire.[12] Neither approach is adequate to model the Raman spectra of highly stressed *polycrystalline* diamond films.

We study here the Raman spectra of highly stressed, polycrystalline, CVD diamond films and develop a model for determining the stress state quantitatively from detailed structure within the Raman spectrum. An analysis is performed of the Raman spectra of diamond deposited on Ti−6Al−4V, a common aircraft alloy with a nominal composition of 5.5–6.75 at. % Al and 3.5–4.5 % Al,[28] and coupled with exploratory work on film adhesion. To measure the adhesion of thin diamond films, a Brale indentation test has been proposed[13,14] which involves penetration of the film and substrate with a hemispherical diamond indenter under a load of 500−1500 N. Although the details of the test with respect to a measurement of adhesion are discussed elsewhere,[15] an elevation of the film stress in the vicinity of the indentation allows for a study of films under exceptionally high residual stress.

II. EXPERIMENT

Polycrystalline diamond films (nominally 1-μm thick) were grown on $60\times20\times3$ mm rectangular substrates of Ti−6Al−4V alloy by microwave plasma CVD processes.[16] The films are weakly (111) oriented as determined from a comparison of x-ray-diffraction measurements in θ-2θ and 2θ-grazing incidence geometries.[5] Film adhesion was evaluated by indenting with a hemispherical Brale C diamond indenter at various points using a range of loads from 588−1470 N. We discuss in detail here the Raman spectra in the vicinity of two indentations produced by a 588-N load and a 980-N load (Figs. 1 and 2). Delaminated and adherent areas can be seen in Fig. 1; in Fig. 2, the film is completely delaminated in the region around the indentation.

Raman measurements were performed with the 488-nm line of an Ar-ion laser focused onto the film with a 65-mm achromat. The laser light was incident at 65° from surface normal; scattered light was collected by an

0163-1829/93/48(4)/2601(7)/$06.00 © 1993 The American Physical Society

$f/1$ 50-mm camera lens normal to the surface. The laser spot size was 10 μm and the sample could be moved in one dimension with a translation stage equipped with a dc motor and encoder with an accuracy of better than 1 μm.

III. RESULTS

The Raman spectrum of the film far away from the indentations ("as-grown" film) is shown in Fig. 3. The broad peak at ca. 1530 cm^{-1} seen in the inset is attributed to a small amount of sp^2-bonded carbon (which has a Raman cross section ca. 50× that of diamond). The feature at ca. 1350 cm^{-1} is two peaks centered at 1352 and 1338 cm^{-1}. As discussed below, the peaks are attributed to the zone-center phonon of diamond (triply degenerate in unstressed diamond) which has been shifted from its normal position at 1332 cm^{-1} and split into two components (doublet at higher frequency and a singlet at lower frequency, cf. below) by the large compressive in-plane stress present in the film.

Raman spectra were collected as a function of position x away from the indentation center in the vicinity of both indentations as shown in Figs. 1 and 2. As indicated in Fig. 1 for the 588-N indentation, one data series was taken across a delaminated region (I) and one data series was taken across an adherent region (II). Representative spectra from scan II are shown in Fig. 4. Figure 4(a) shows the Raman spectrum of unstressed material (single Raman peak at 1332 cm^{-1}) obtained at the indent edge $x/r=1$ where r is the indentation radius. Identical spectra were obtained from delaminated material in scans I and III. Figure 4(c) shows the Raman spectrum from a point 1000 μm ($x/r=5.5$) from the 588-N indentation; the spectrum has peaks at 1352 and 1338 cm^{-1} and is essentially identical to that of the as-grown film shown in Fig. 3. Figure 4(b) shows the Raman spectrum a point close to the 588-N indentation ($x/r=2$); the spectrum is different than that of the as-grown film [Figs. 3 and 4(c)] with peaks at 1376 and 1348 cm^{-1}, indicating that the film has an additional residual stress component due to the indentation.

(a)

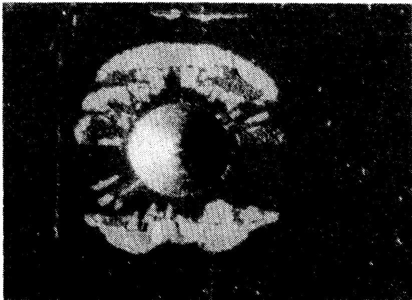

(b)

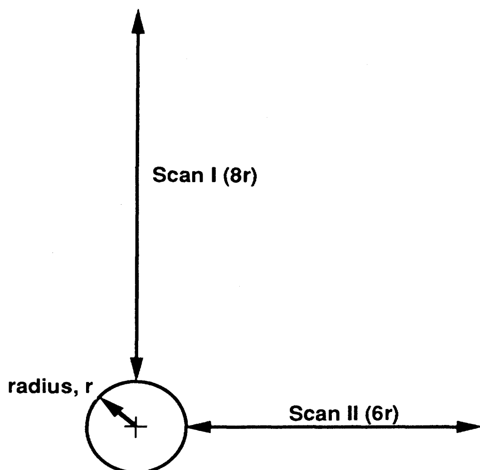

FIG. 1. Optical micrograph (a) of indented CVD diamond film on Ti–6Al–4V at 588 N (indentation radius, $r=222$ μm) and (b) directions of Raman measurements (scans I and II).

(a)

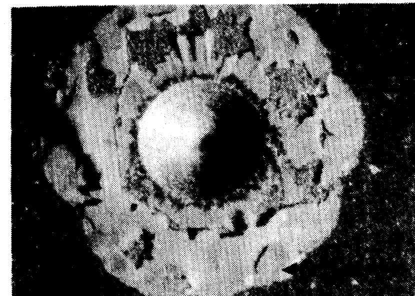

(b)

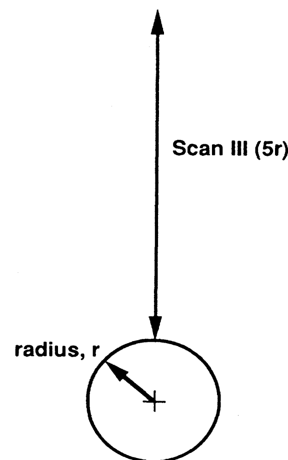

FIG. 2. Optical micrograph (a) of indented CVD diamond film on Ti–6Al–4V at 980 N (indentation radius, $r=290$ μm) and (b) direction of Raman measurements (scan III).

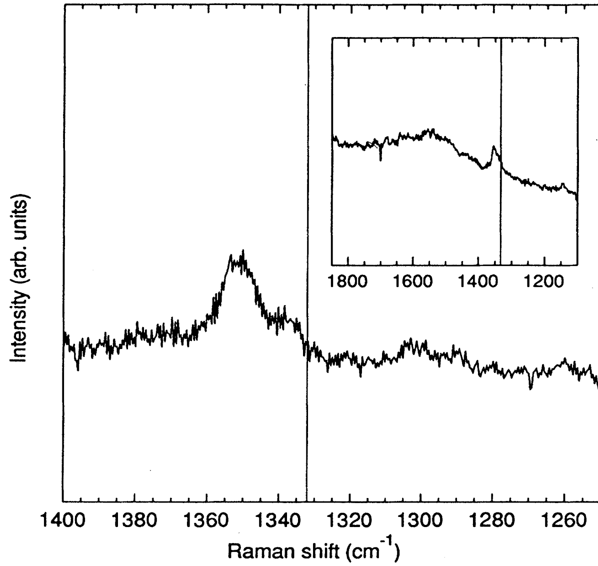

FIG. 3. Raman spectrum of CVD diamond grown on Ti–6Al–4V (as-grown film, no indentation) at 3 cm^{-1} and parallel polarization. The inset shows a lower resolution spectrum (6 cm^{-1}) with a broad feature at ca. 1500 cm^{-1} which is attributed to a small amount of amorphous carbon. The vertical lines indicate the Raman frequency of stress-free diamond, 1332 cm^{-1}.

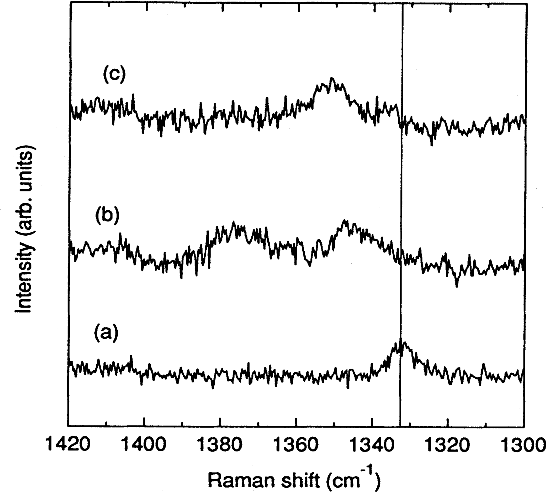

FIG. 4. Raman spectra in the vicinity of the indentation shown in Fig. 1, scan II: (a) $x/r=1$ (at indent edge), zero residual stress; (b) $x/r=2$—the splitting of the doublet peak indicates a highly stressed state; (c) $x/r=5.5$, doublet and singlet peak observed, 7.1-GPa biaxial residual compressive stress, same as in as-grown film. The vertical line indicates the Raman frequency of unstressed diamond, 1332 cm^{-1}.

IV. DISCUSSION

Examination of spectra obtained in areas of high residual stress near the indentation indicates that there may be three or more identifiable spectral components whose frequencies vary with distance from the indentation. For simplicity, and to provide an estimate of the magnitude of the residual stress field surrounding the indents, only the Raman frequency of the highest-frequency component is graphed as a function of position in Figs. 5 and 6. Nevertheless, a few simple observations can be made: (1) delaminated material is stress free with Raman frequency of 1332 cm^{-1}; (2) for $x/r>$ ca. 5.5, the Raman spectrum is that of the as-grown film; and (3) a region of elevated stress is found at $1.5<x/r<2.5$. The elevated residual stress appears to have caused film delamination in scan I between $x/r=0.8$ and 2.0 (with a small region of adhering film at $x/r=1.2$) and in scan III between $x/r=1$ and 2.5 and at $x/r=2.8$. The indentation stress appears to have taken up in the film in scan II, leading to a very high observed Raman frequency, 1376 cm^{-1}, at $x/r=2$.

Raman spectroscopy has been used to measure stress quantitatively in thin films of diamond and zinc-blende-structure films used in prototype electronic devices[17–21] and in strained-layer superlattices.[22] The basis for the previous work has been the measurement of the Raman spectrum of diamond and zinc-blende-structure materials under uniaxial[22] and hydrostatic stress conditions,[23] which can be used to determine the "phonon deformation potentials," and which relate the shift and splitting of the zone-center optical phonons to strains along crystallographic axes. The phonon deformation potentials can be used to predict the Raman spectrum for a given strain and crystallographic orientation. The converse problem of calculating the strain and stress tensors is more difficult for unknown stress directions, as discussed below.

The Raman spectrum is analyzed here by developing the theory of the shift and splitting of three degenerate (at zero stress) components of the zone-center optical phonon in a cubic material. Consideration of the dynamical equations under small strains yields the following secular equation whose solution determines the shift of the Raman phonons:[24,25]

$$\begin{vmatrix} p\varepsilon_{xx}+q(\varepsilon_{yy}+\varepsilon_{zz})-\lambda & 2r\varepsilon_{xy} & 2r\varepsilon_{xz} \\ 2r\varepsilon_{xy} & p\varepsilon_{xx}+q(\varepsilon_{xx}+\varepsilon_{zz})-\lambda & 2r\varepsilon_{yz} \\ 2r\varepsilon_{xz} & 2r\varepsilon_{yz} & p\varepsilon_{zz}+q(\varepsilon_{xx}+\varepsilon_{yy})-\lambda \end{vmatrix}=0\ , \tag{1}$$

where $\lambda=\Omega^2-\omega_0^2$, simplified as $\lambda\approx 2\omega_0(\Omega-\omega_0)$ for small shifts, and x, y, and z are the crystallographic axes [100], [010], and [001], respectively. The shifted and unshifted Raman frequencies, Ω and ω_0, are in angular units. The phonon deformation potentials p, q, and r are related to changes in spring constants with applied strain[24] and have been measured for many cubic materials,[22] including diamond.[26]

Analytical solutions to Eq. (1) are available for uniaxial stress along ⟨100⟩ and ⟨111⟩ axes[24] and for biaxial strain in {100} planes.[12] The general method for obtaining the shifts for an arbitrary stress state is outlined here with particular emphasis on the biaxial (in-plane) stress expected for diamond growth. The method involves expressing the stress tensor referenced to a convenient set of axes, rotating to a stress tensor referenced to x, y, and z, calculating the strains ε_{ij} $(i,j=x,y,z)$, and solving Eq. (1) for the phonon frequencies. Calculations of the biaxial stress in the (111) plane are given in the Appendix. For diamond, biaxial compressive stress in either {100} or {111} planes splits the Raman phonon into a singlet and a doublet (wave vector perpendicular and parallel to stress plane, respectively); the doublet is at higher frequency in diamond. Biaxial stresses along other axes splits the triple degeneracy completely.

Relating the observed Raman spectrum to the residual stress state is more complicated than in previous studies of strain in epitaxial layers, because in the present case neither the stress nor the crystal orientation are known *a priori*, particularly in the immediate vicinity of the indentations. Nevertheless, quantitative results can be obtained when $x \gg r$, where x is the distance from the indentation center and r is the indentation radius, by making a few reasonable assumptions: (1) that the stress is primarily biaxial and in the plane of the film, and (2) that the polycrystalline nature of the film allows both doublet and singlet Raman modes to be observed in backscattering from most crystal orientations. In a single crystal, only the singlet can be observed in backscattering from {100}, while both the singlet (parallel polarization) and doublet (perpendicular polarization) are observed in backscattering from {100} and $\{11\bar{2}\}$.[24] The polarized Raman spectra of the as-grown film (Fig. 7) show an increase in intensity of the higher frequency peak in perpendicular polarization. This observation supports assignment of this peak to the doublet modes of grains of various orientations.

Using the diamond phonon deformation potentials and compliance constants in Table I and Eqs. (A4) and (A5), the biaxial stresses corresponding to singlet and doublet phonon frequencies are the following:

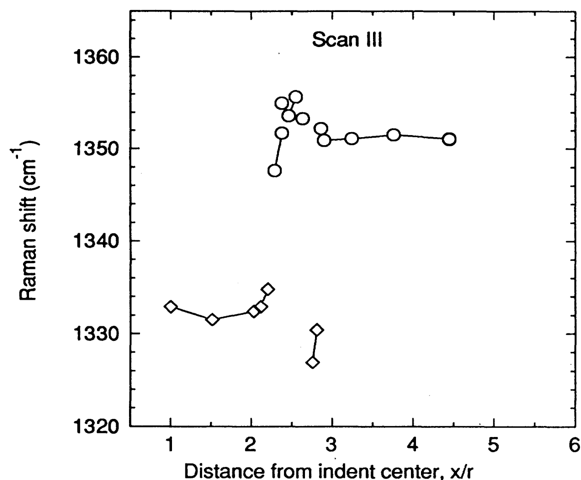

FIG. 6. Raman frequency of the highest-frequency spectral component (see text) vs position x (in units of indentation radius) for the 980-N indentation (scan III).

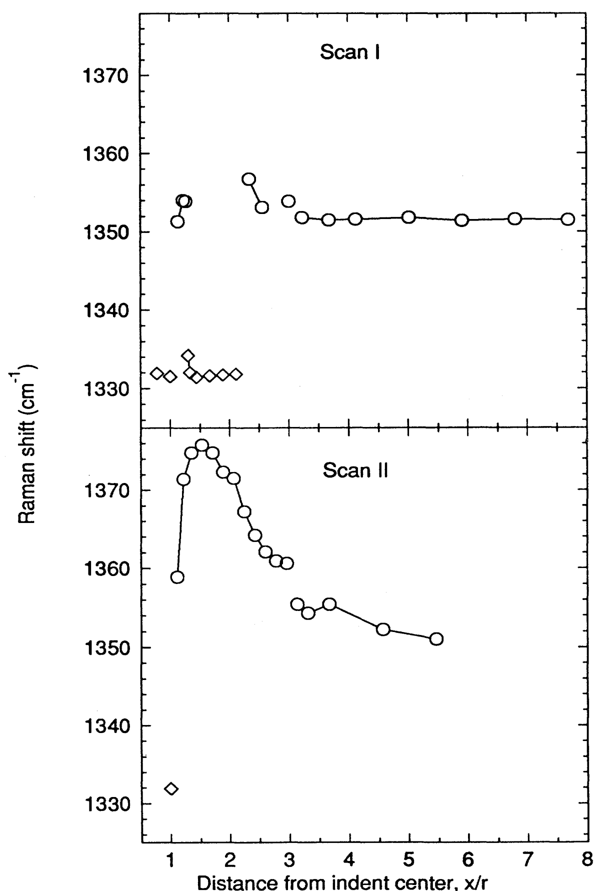

FIG. 5. Raman frequency of the highest-frequency spectral component (see text) vs position x (in units of indentation radius) for the 588-N indentation (scans I and II).

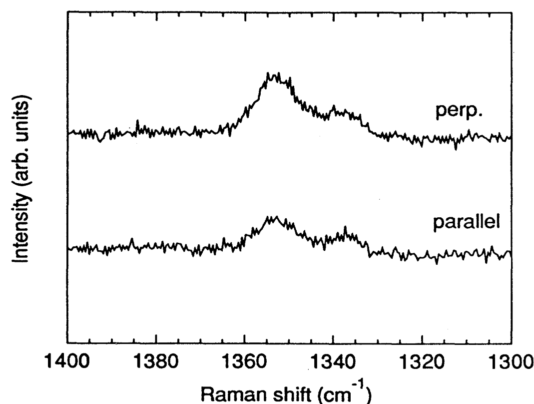

FIG. 7. Polarized Raman spectra from as-grown film. The spectrum has been normalized and offset for clarity.

TABLE I. Parameters used in the stress calculation.

Strain parameters ($\times 10^{-28}$ s^{-2})		
p	−17.2	Ref. 26
q	−11.2	
r	−12.0	
Compliance constants ($\times 10^{-14}$ dyn cm^{-2})		
s_{11}	9.524	Ref. 27
s_{12}	−0.9913	
s_{44}	17.36	

$$\tau = -0.610\ \text{GPa/cm}^{-1}(\nu_s - \nu_0) \quad \text{for the (100) singlet}, \tag{2a}$$

$$\tau = -0.422\ \text{GPa/cm}^{-1}(\nu_d - \nu_0) \quad \text{for the (100) doublet}, \tag{2b}$$

$$\tau = -1.49\ \text{GPa/cm}^{-1}(\nu_s - \nu_0) \quad \text{for the (111) singlet}, \tag{2c}$$

$$\tau = -0.350\ \text{GPa/cm}^{-1}(\nu_d - \nu_0) \quad \text{for the (111) doublet}, \tag{2d}$$

where ν, the observed maxima in the spectrum, are in wave-number units, and $\nu_0 = 1332$ cm^{-1}. Values for biaxial stress in (110) and $(11\bar{2})$ planes are obtained by following the procedure in the Appendix and solving Eq. (1) numerically,

$$\tau = -1.11\ \text{GPa/cm}^{-1}(\nu_s - \nu_0) \quad \text{for the (110) singlet}, \tag{3a}$$

$$\tau = -0.444\ \text{GPa/cm}^{-1}(\nu_d - \nu_0) \quad \text{for the (110) doublet}, \tag{3b}$$

$$\tau = -1.11\ \text{GPa/cm}^{-1}(\nu_s - \nu_0) \quad \text{for the } (11\bar{2}) \text{ singlet}, \tag{3c}$$

$$\tau = -0.357\ \text{GPa/cm}^{-1}(\nu_d - \nu_0) \quad \text{for the } (11\bar{2}) \text{ doublet}, \tag{3d}$$

where the split doublet values have been averaged. Using the average of the above singlet and doublet values [excluding the (100) doublet value since Raman scattering from the phonon is forbidden in backscattering] yields the following equations for biaxial stress in a polycrystalline diamond film:

$$\tau = -1.08\ \text{GPa/cm}^{-1}(\nu_s - \nu_0) \quad \text{for the singlet phonon}, \tag{4a}$$

$$\tau = -0.384\ \text{GPa/cm}^{-1}(\nu_d - \nu_0) \quad \text{for the doublet phonon}. \tag{4b}$$

Equation (4) yields reasonably consistent in-plane stress values of 6.5 and 7.7 GPa from the maxima of the singlet (1338 cm^{-1}) and the doublet (1352 cm^{-1}) observed in the Raman spectrum of the as-grown material.

Stick spectra calculated using Eqs. (2) and (3) and the average of the above values, 7.1 GPa, are shown in Fig. 8. The stick spectra correspond well to the observed Raman spectrum of the as-grown film (also shown in Fig. 8), indicating that the observations are modeled well by the present biaxial stress model. The observed spectrum would not be fit well by using only the values for (100) in-plane stress, i.e., if the approach of Ref. 12 were used to interpret the present data.

Thermal stress can be readily estimated by

$$\sigma_{\text{thermal}} = \frac{E}{1-\nu} \int_{20\,^\circ\text{C}}^{T} (\alpha_f - \alpha_s)\, dT, \tag{5}$$

where E is Young's modulus of diamond, $1/s_{11}$ or 1050 GPa, α_f and α_s are the thermal-expansion coefficients of the film and substrate [9.5×10^{-6}/K for Ti–6Al–4V and 0.8×10^{-6}/K for diamond at room temperature]; ν (=0.07) is the Poisson ratio of the film, and T, 900 °C, is the growth temperature. Equation (5) predicts a compressive film stress of 6.8 GPa, which is in excellent agreement with the measured value. Therefore, the very large measured stress in the film is consistent with the thermal-expansion mismatch of the diamond film and the substrate.

The data in Figs. 5 and 6 show that the stress state of the film is changed close to the indentations. In addition, there is evidence that the stress state near the indentation is not biaxial. We tentatively assign the two peaks of approximately equal intensity in Fig. 4(b) to a split doublet peak, the lower-frequency component of which overlaps

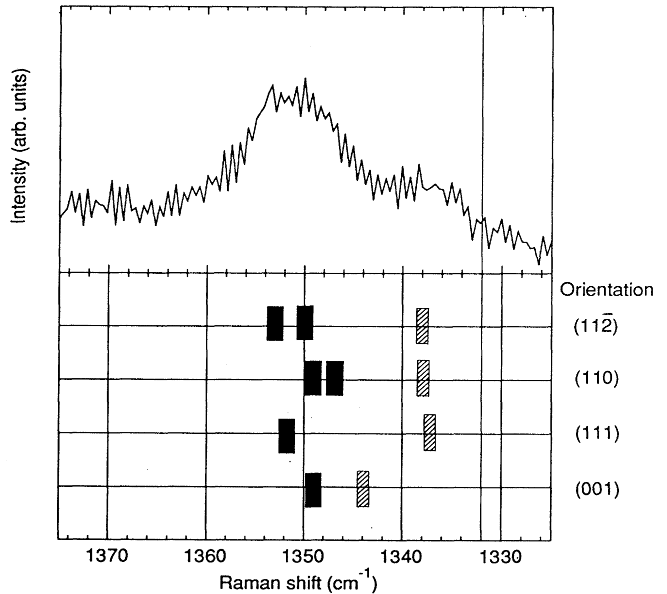

FIG. 8. Calculated stick spectra for 7.1-GPa biaxial stress in the four indicated crystallographic planes (bottom) and observed as-grown Raman spectrum (top). The solid bars represent the doublet frequencies and the hatched bars represent the singlet frequencies.

the singlet peak. Analysis of the spectrum, perhaps in crystallographically oriented films, may be able to resolve the hoop and radial components of the stress field expected in the vicinity of the indentation. As a very crude approximation, using Eq. (4b), it is possible to estimate the maximum stress (assuming that it is still biaxial) at the point of maximum residual stress, $x/r=2$ in scan II. The observed peak position of 1376 cm^{-1} of the high-frequency peak corresponds to 17 GPa of residual stress. Elevation of the residual stress in the vicinity of the indentation is consistent with the additional (residual) load provided by the plastically deformed substrate.[15]

V. CONCLUSIONS

Promising initial results on the quantitative measurement of residual stress with Raman spectroscopy are presented. The method presented here will enable a more critical examination of the effects of residual stress on film adhesion in polycrystalline, diamond-structure materials. The large residual in-plane stress, 7.1 GPa, observed in polycrystalline diamond on Ti–6Al–4V is attributed to thermal-expansion mismatch. The magnitude of the residual stress is larger than previously reported values on other substrates. Examination of the Raman spectra of the film in the vicinity of Brale indentations reveals that residual stresses in the film of up to approximately 17 GPa can be accommodated in the film before delamination occurs. This suggests very strong interface bonding, possibly due to the formation of carbides in the interface region. The origins of the strong interface bonding will be explored in future work.

ACKNOWLEDGMENTS

This work was supported by the Director, Office of Energy Research, U.S. Department of Energy, under Contract No. DE-AC03-76SF00098 (J.W.A.).

APPENDIX

The analytical calculation of the shift of the Raman phonons of a cubic material under $\langle 111 \rangle$-plane stress is presented. We begin by defining a second set of axes, x'', y'', and z'' which are parallel to $[11\bar{2}]$, $[\bar{1}10]$, and $[111]$, respectively, by using the notation of Ref. 24. A biaxial, in-plane stress, τ in the [111] plane referred to these axes is expressed as[12]

$$\sigma''=\tau\begin{bmatrix}1&0&0\\0&1&0\\0&0&0\end{bmatrix} . \tag{A1}$$

Rotating to x,y,z basis yields the stress tensor

$$\sigma=\tau\begin{bmatrix}\frac{2}{3}&-\frac{1}{3}&-\frac{1}{3}\\-\frac{1}{3}&-\frac{2}{3}&-\frac{1}{3}\\-\frac{1}{3}&-\frac{1}{3}&\frac{2}{3}\end{bmatrix} , \tag{A2}$$

and calculating the strains using Hooke's law, $\varepsilon_i=S_{ij}\tau_j$, where $(i,j=1,2,\ldots,6)$ (see Ref. 29 for an explanation of the single subscript notation), yields

$$\varepsilon_{xx}=\varepsilon_{yy}=\varepsilon_{xx}=\tfrac{2}{3}(s_{11}+2s_{12})\tau , \tag{A3a}$$

$$\varepsilon_{xx}=\varepsilon_{yz}=\varepsilon_{xy}=-1/6s_{44}\tau . \tag{A3b}$$

Solution of the secular equation (1) with these strains yields:

$$\Omega_s=\omega_0+\frac{\tau}{2\omega_0}[\tfrac{2}{3}(p+2q)(s_{11}+s_{12})-2/3rs_{44}] , \tag{A4a}$$

$$\Omega_d=\omega_0+\frac{\tau}{2\omega_0}[\tfrac{2}{3}(p+2q)(s_{11}+s_{12})+1/3rs_{44}] . \tag{A4b}$$

A similar analysis for biaxial stress in (001) yields[12]

$$\Omega_s=\omega_0+\frac{\tau}{2\omega_0}[2ps_{12}+2q(s_{11}+3s_{12})] , \tag{A5a}$$

$$\Omega_d=\omega_0+\frac{\tau}{2\omega_0}[2ps_{12}+2q(s_{11}+s_{12})] . \tag{A5b}$$

*Also at Crystallume, 125 Constitution Ave., Menlo Park, CA 94025.

[1]W. A. Yarbrough and R. Messier, Science **247**, 688 (1990).
[2]J. C. Angus and C. C. Hayman, Science **241**, 913 (1988).
[3]K. E. Spear, J. Am. Ceram. Soc. **72**, 171 (1989).
[4]*Thin Films: Stresses and Mechanical Properties III,* MRS Symposia Proceedings No. **239** (Materials Research Society, Pittsburgh, 1991).
[5]H. Windischmann, G. F. Epps, Y. Cong, and R. W. Collins, J. Appl. Phys. **69**, 2231 (1991).
[6]D. S. Knight and W. B. White, J. Mater. Res. **4**, 385 (1989).
[7]A. G. Evans, M. D. Drory, and M. S. Hu, J. Mater. Res. **3**, 1043 (1988).
[8]J. A. Baglio, B. C. Farnsworth, S. Hankin, G. Hamill, and D. O'Neil, Thin Solid Films **212**, 180 (1992).
[9]B. S. Berry, W. C. Pritchet, J. J. Cuomo, C. R. Guarnieri, and S. J. Whitehair, Appl. Phys. Lett. **57**, 302 (1990).
[10]M. Yoshikawa, H. Ishida, A. Ishitani, T. Murakami, S. Koizumi, and T. Inuzuka, Appl. Phys. Lett. **57**, 428 (1990).
[11]W. Wanlu, L. Kejun, G. Jinying, and L. Aimin, Thin Solid Films **215**, 174 (1992).
[12]T. Englert, G. Absteiter, and P. Pontcharra, Solid State Electron. **23**, 31 (1980).
[13]P. K. Mehrotra and D. T. Quinto, J. Vac. Sci. Technol. A **3**, 2401 (1985).
[14]T.-Y. Yen, C.-T. Kuo, and S. Hsu, Mat. Res. Soc. Proc. **168**, 207 (1990).
[15]M. D. Drory *et al.* (unpublished).
[16]S. S. Perry, J. W. Ager III, G. A. Somorjai, R. J. McClelland, and M. D. Drory (unpublished).
[17]I. H. Campbell, P. M. Fauchet, E. H. Lee, and M. A. Awal, Thin Solid Films **154**, 249 (1987).

[18]L. E. Trimble, G. K. Celler, D. G. Schimmel, C. Y. Lu, S. Nakahara, and P. M. Fauchet, J. Mater. Res. **3**, 514 (1988).
[19]S. A. Lyon, R. J. Nemanich, N. M. Johnson, and D. K. Biegelsen, Appl. Phys. Lett. **40**, 316 (1982).
[20]I. DeWolf, J. Vanhellemont, A. Romero-Rodríguez, H. Norström, and H. E. Maes, J. Appl. Phys. **71**, 898 (1992).
[21]H. Shen and F. H. Pollak, Appl. Phys. Lett. **45**, 692 (1984).
[22]B. Jusserand and M. Cardona, in *Light Scattering in Solids V*, edited by M. Cardona (Springer, New York, 1988), p. 127.
[23]B. A. Weinstein and R. Zahlen, in *Light Scattering in Solids IV*, edited by M. Cardona (Springer, New York, 1984).
[24]E. Anastassakis, A. Pinczuk, E. Burstein, F. H. Pollak, and M. Cardona, Solid State Commun. **8**, 133 (1970).
[25]P. Wickboldt, E. Anastassakis, R. Sauer, and M. Cardona, Phys. Rev. B **35**, 1362 (1987).
[26]M. H. Grimsditch, E. Anastassakis, and M. Cardona, Phys. Rev. B **18**, 901 (1978).
[27]M. H. Grimsditch and A. K. Ramdas, Phys. Rev. B **11**, 3139 (1975).
[28]*Metals Handbook—Properties and Selection: Stainless Steels, Tool Materials, and Special-Purpose Metals,* 9th ed., edited by ASM Handbook Committee (American Society for Metals, Metals Park, OH, 1980), Vol. 3, pp. 388–390.
[29]J. F. Nye, *Physical Properties of Crystals* (Clarendon, Oxford, 1957), pp. 150–169.

(a)

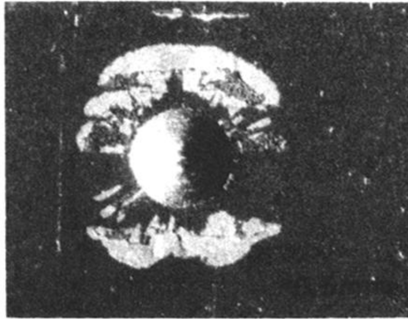

(b)

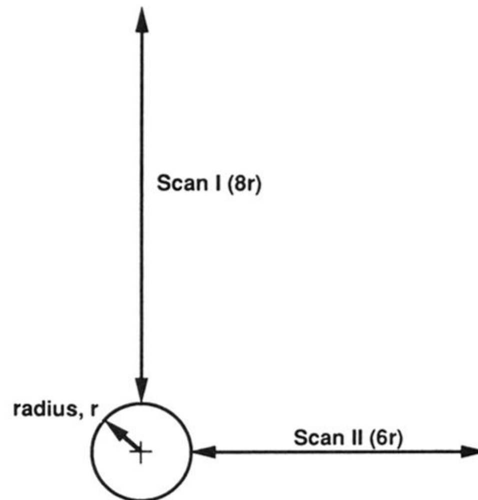

FIG. 1. Optical micrograph (a) of indented CVD diamond film on Ti–6Al–4V at 588 N (indentation radius, $r = 222\ \mu m$) and (b) directions of Raman measurements (scans I and II).

(a)

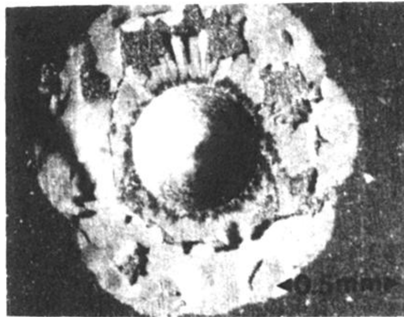

(b)

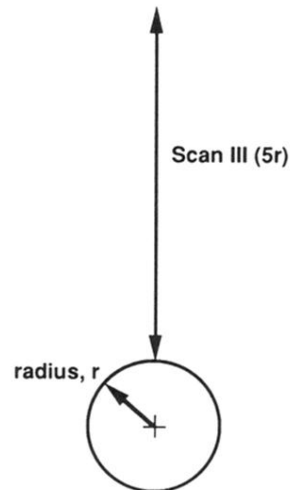

FIG. 2. Optical micrograph (a) of indented CVD diamond film on Ti–6Al–4V at 980 N (indentation radius, $r=290\ \mu m$) and (b) direction of Raman measurements (scan III).